with different relaxation frequencies must be present in the temperature range near 24.6 K (Figure 11). At 23.1 K this appears only in asymmetric lines. Between 24 and 26 K, however, there appears in addition—as mentioned above—a central asymmetric double due to faster relaxation that is still observable up to 42 K (see Figures 11 and 12). With equal relaxation rates for the three Fe positions in the compound with $x = 0.50$, we can fit the spectra very well. We also analyzed the spectra with different flip rates but were unable to obtain a better agreement with the data.

In Figure 13, we show the spin-flip rate for $x = 0.01$ and $x = 0.50$. The straight lines show the exponential dependence on reciprocal temperature, characteristic for an activated soliton process $W = \exp(-E_A/kT)$.[6] The calculated activation energies E_A/k are 217 (5) and 124 (5) K for $x = 0.01$ and $x = 0.50$, respectively. If the temperature-independent texture effect mentioned above is considered, the activation energy E_A/k derived from Mössbauer experiments corresponds to 234 (15) K for $x = 0.01$. The temperatures at which the drop of the flip rates occurs in Figure 13 correspond to 26.5 and 17.0 K. One may interpret this as a blocking of the domain wall motion by the 3-D long-range order. The 3-D ordering points are a few degrees lower. For $x = 0.50$, we determined the value of T_N to be 14.5 (1.0) K from susceptibility measurements (see Table I).

With decreasing Mn(III) concentration and easy-axis anisotropy energy, the activation energy is reduced by a factor of about 2 for $x = 0.50$. This is consistent with the results for $Rb_2FeF_5 \cdot H_2O$. As can be seen from Figure 2b as reported by Fourquet et al.,[11] the spectra above the 3-D phase transition do not display any temperature-dependent line broadening. Solitons are present by virtue of the anisotropy, and for the Fe(III) system, the anisotropy energy will probably be smaller than the 3-D ordering energy kT_N. The trend of the activation energy obtained from the Mössbauer experiments is so far quite convincing. Such a decrease of the activation energy with decreasing anisotropy energy may be understood from the classical domain wall theory (for review see ref 8)

$$E_s = 2\pi S^2(D \cdot J)^{1/2} \quad (3)$$

where E_s represents the creation energy of solitons. This approximation may be convenient if the spin value is large, so that the classical spin vector is approached, and if the characteristic wavelengths of the fluctuations in the spin system (e.g. the widths of the solitons) are large compared to the lattice spacing. Assuming that the classical domain wall theory is also valid in our case of a random system and inserting in eq 3 the experimental values of J_{FeMn} (as an averaged value of J), $E_s = E_A$ and the average spin of the solid solutions, we can estimate the anisotropy constants $D = E_A^2/(4\pi^2 S^4 J)$ to be equal to 3.0 (3) and 1.0 (3) K for $x = 0.01$ and $x = 0.50$, respectively. The value of the anisotropy constant for $x = 0.01$ is in fair agreement with the D values derived from magnetic susceptibility measurements on single crystals of the related solid solutions $(NH_4)_2Mn_{1-x}Fe_xF_5$ with $x = 0$ and $x = 0.02$[17,18] mentioned above. the preliminary results on $(NH_4)_2Mn_{0.55}Fe_{0.45}F_5$ seem to confirm such a decrease of D with increasing Fe content. unfortunately, however, the magnetic structure, apparently important for establishing this correlation, is more complex than those derived for the lowest x values. Therefore, a Mössbauer and neutron diffraction study on powder samples and a study of the magnetic susceptibility on single crystals of $(NH_4)_2Mn_{1-x}Fe_xF_5$ up to $x = 0.60$ are now under investigation.[18]

Acknowledgment. I am indebted to J. L. Soubeyroux (ILL, Grenoble, France) for the neutron diffraction experiment. I am also indebted to J. M. Dance for the g factor measurement. The financial support of the Commission of the European Community is gratefully acknowledged.

Contribution from the Fachbereich Chemie
der Philipps-Universität, D-3550 Marburg/Lahn, FRG

Color and Electronic Structure of Manganese(V) and Manganese(VI) in Tetrahedral Oxo Coordination. A Spectroscopic Investigation

Herbert Lachwa and Dirk Reinen*

Received July 29, 1988

From the single-crystal EPR spectra of Mn(V) in tetrahedral oxo coordination in the compounds $Ca_2(MO_4)Cl$ [M = P(V), V(V), As(V)] with the spodiosite structure are derived the ground-state electronic structure and the geometry and orientation of the MnO_4 polyhedra in the host lattice, and the obtained zero-field-splitting parameters are compared with those from powder EPR spectra of various other oxo compounds. In the case of M = P(V), where a considerable mismatch between the volume of the doped and the host polyhedra exists, the MnO_4^{3-} entities are flattened to a greater extent than the PO_4^{3-} tetrahedra and also the axis of compression has a slightly different orientation. The reflectance spectra are assigned with respect to the d–d and charge-transfer transitions on the basis of literature data and related to the color properties. The correlation of the color shift from green to blue of the prepared Mn(V) compounds with the host site geometry, the chemical constitution, and the Mn(V) concentration is discussed. Finally, a comparison with corresponding spectral data for Mn(VI) is made.

Introduction

Intensive and bright colors are observed if transition-metal ions are incorporated into the tetrahedral sites of solid host compounds. Manganese(V) can be stabilized in tetraoxo coordination by isomorphous substitution in phosphate compounds and induces blue or green colors.[1-4] Recently, the first single-crystal X-ray structure investigation of a Mn(V) compound, namely $Ba_5(MnO_4)_3Cl$, which crystallizes in the apatite structure, was performed.[4] The stability of Mn(V) is strongly dependent on the simultaneous presence of cations with pronounced base properties. The mixed crystals $A^{II}_5(PO_4)_{3-x}(MnO_4)_xX$ (X = Cl^-, OH^-, F^-) can be synthesized over the whole range of x values for $A^{II} = Ba^{2+}$, with color variations from light blue at very low Mn(V) concentrations through turquoise-blue and green to dark green for $x = 3$ (Figure 1). The corresponding compounds with Sr^{2+} and Ca^{2+} are only stable up to $x = 1.5$ and $x = 0.1$, respectively, and are blue at low doping concentrations.[4] Single-crystal electronic spectra of tetrahedral Mn(V) in host lattices with the apatite and spodiosite structure and band assignments are reported by Day et al.[5] and Milstein and Holt.[6] Electronic reflection and powder EPR data, which were analyzed with respect to the zero-field splitting pa-

(1) Lux, H. *Z. Naturforsch.* **1946**, *1*, 281.
(2) Klemm, W. *Angew. Chem.* **1954**, *66*, 468. Krause, J. Dissertation, University of Münster, 1954.
(3) Scholder, R. *Angew. Chem.* **1954**, *66*, 461.
(4) Reinen, D.; Lachwa, H.; Allmann, R. *Z. Anorg. Allg. Chem.* **1986**, *542*, 71.
(5) Borromei, R.; Oleari, L.; Day, P. *J. Chem. Soc., Faraday Trans.* **1977**, *73*, 135; **1981**, *77*, 1563.
(6) Milstein, J.; Holt, S. L. *Inorg. Chem.* **1969**, *8*, 1021.

0020-1669/89/1328-1044$01.50/0

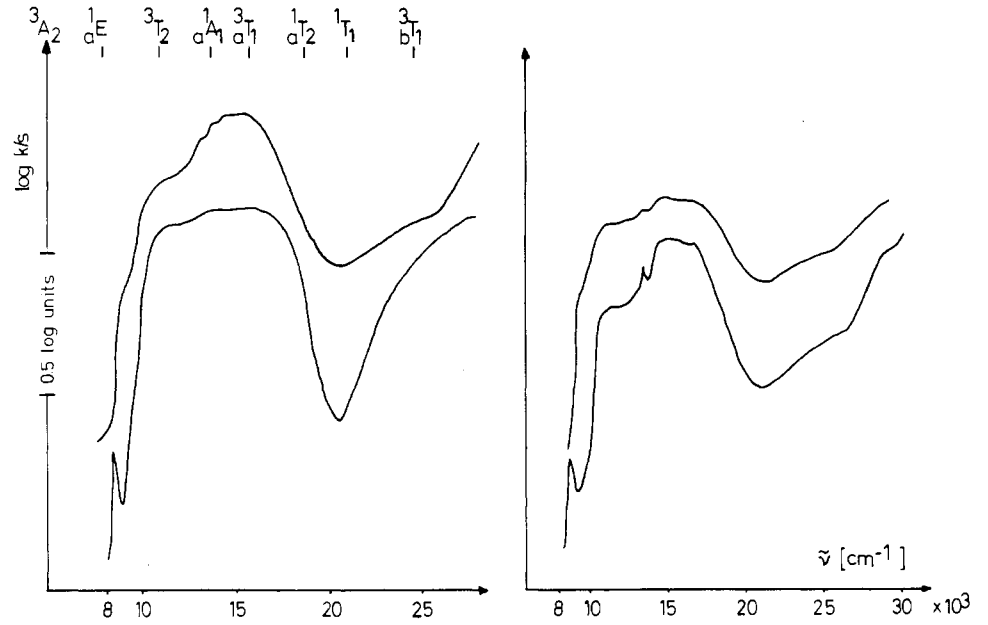

Figure 1. Reflection spectra of Mn(V) in apatite-type mixed crystals: (left) $Ba_5(PO_4)_{3-x}(MnO_4)_xCl$ (298 K) with $x = 0.05$ (above) and $x = 1.0$ (below); (right) $Sr_5(PO_4)_{2.9}(MnO_4)_{0.1}Cl$ at 298 K (above) and 5 K (below). Band assignments refer to T_d symmetry, and transition energies were calculated with the parameters $\Delta = 11\,000$ cm^{-1}, $B = 500$ cm^{-1}, and $C/B = 4.0$.

rameters, of the just mentioned apatite mixed crystals have also been published.[4]

This study gives results from single-crystal EPR investigations of Mn(V) in spodiosite- and apatite-type host lattices and from EPR and electronic powder spectra of various oxo compounds with tetrahedral Mn(V) and Mn(VI). It is expected to yield the following information: (1) the symmetry of the Mn coordination and the electronic structure of the ground state; (2) correlations between the structure and composition of the host lattice as well as the Mn concentration and the color variations and band shifts in the electronic spectra; (3) criteria to distinguish between Mn(V) and Mn(VI).

Experimental Section

A. Preparation and X-ray Characterization. The preparation of manganese(V) compounds with the apatite structure is described elsewhere.[4] Mn(V)-doped single crystals were obtained by heating the powders in an excess of $BaCl_2$ ($SrCl_2$) in sealed platinum capsules for 10 h at temperatures of 1000 °C (900 °C) and successive cooling with a rate of 12.5 °C/h. $BaCl_2$ ($SrCl_2$) was removed from the solid melt with hot water. Spodiosite-type mixed crystals of the composition $E^{II}_2(M^V_{1-x}Mn^V_xO_4)Cl$ (E^{II} = Ca, Sr; M^V = P, V, As) were prepared by the method of Kingsley et al.[7] Single crystals resulted from the melts when excess of $SrCl_2$ ($CaCl_2$) in platinum crucibles or in sealed platinum capsules was applied, as described above (annealing temperature 900 °C (800 °C)). Sr spodiosites with M^V = P, As could not be synthesized because the corresponding apatite phases were always obtained. The limit of Mn(V) substitution in the M^V position was ≈2 mol % (see below). The blue single crystals (powdered material) had the following unit cell dimensions (space group *Pbcm*):

	a, Å	*b*, Å	*c*, Å
$Ca_2(PO_4)Cl$	6.192	7.002	10.841
$Ca_2(VO_4)Cl$	6.303	7.134	11.046
$Ca_2(AsO_4)Cl$	6.346	7.118	11.064
$Sr_2(VO_4)Cl$	6.531	7.542	11.050

Mn(V)-doped Li_3VO_4 and Li_3AsO_4 were prepared by heating mixtures of $V_2O_5(As_2O_3)$, Li_2CO_3, and Mn_2O_3 in air, adding a small amount of LiOH, at 800 °C for a period of 5 h, and cooling slowly. The corresponding phosphates were obtained analogously from a mixture of Li_3PO_4, Li_2CO_3, and Mn_2O_3. The mixed-crystal series $Li_3(PO_4)_{1-x}(MnO_4)_x$ was synthesized in a LiOH melt at 450 °C because higher Mn(V) concentrations in the host matrix could only be stabilized at low temperatures. The compounds were obtained in the high- or low-temperature structure, depending on the preparation conditions (see below).

Table I. Geometries of MO_4 Polyhedra in Apatite-Type Compounds $E_5(MO_4)_3Cl$ (Space Group $P6_3/m$) (E, M: Sr, P;[10] Ba, P;[11] Ba, Mn[4])[a]

	E, M		
	Sr, P	Ba, P	Ba, Mn
	M–O Spacings (Å)		
M–O1	1.540 (2)	1.548 (8)	1.695 (10)
M–O2	1.544 (2)	1.539 (9)	1.694 (10)
M–O3 (2×)	1.537 (2)	1.536 (7)	1.702 (10)
	O(*i*)–M–O(*j*) Angles 2θ (deg)		
O1–M–O2	111.0 (1)	109.4 (6)	112.6 (6)
O1–M–O3	111.6 (1)	111.8 (3)	112.8 (4)
O2–M–O3	107.0 (1)	107.8(3)	106.0 (4)
O3–M–O3′	108.6 (2)	108.2 (4)	106.0 (6)
δ	1.9 (1)	1.6 (4)	3.4 (5)°

[a] Average deviation from tetrahedral angle $2\theta_t$:

$$\delta = \tfrac{1}{6}\sum_{i=1}^{i=6}|2\theta_i - 2\theta_t|$$

B. Spectroscopic Measurements. The diffuse-reflectance spectra between 4000 and 25 000 cm^{-1} at 298 and 5 K as well as the solution spectra have been recorded on a Zeiss PMQ II spectrophotometer (with a low-temperature accessory). MgO was used as standard. The reflectance data were transformed into log (k/s) values (k and s are absorption and scattering coefficient, respectively) according to the theory of Kubelka-Munk.[8] Only relative intensity scales are given. The EPR measurements between 298 and 4.2 K were performed with a Varian E 15 spectrometer at X- and Q-band frequencies. DPPH was used as internal standard.

Results and Discussion

A. Electronic Spectra. Manganese(V). It is well established[5] that in the electronic spectra of tetraoxo-coordinated Mn(V) charge-transfer bands appear only above 30 000 cm^{-1}. Because, from the three main transitions $^3A_2 \rightarrow {}^3T_2$, $_a{}^3T_1$, $_b{}^3T_1$, the first is symmetry-forbidden in T_d symmetry and the third corresponds approximately to a two-electron jump, only one band of dominating intensity appears (Figures 1–3). Usually two spin-forbidden transitions are also resolved. In Figure 2 the solution spectrum of the blue MnO_4^{3-} entity is shown, in agreement with published data.[9] Figure 1 illustrates the dependence of the d–d spectra of

(7) Kingsley, J. D.; Prener, J. S.; Segall, B. *Phys. Rev.* **1965**, *137A*, 189.
(8) Kubelka, P.; Munk, F. *Z. Tech. Phys.* **1931**, *12*, 593.
(9) Carrington, A.; Symons, M. C. R. *J. Chem. Soc.* **1956**, 3373.

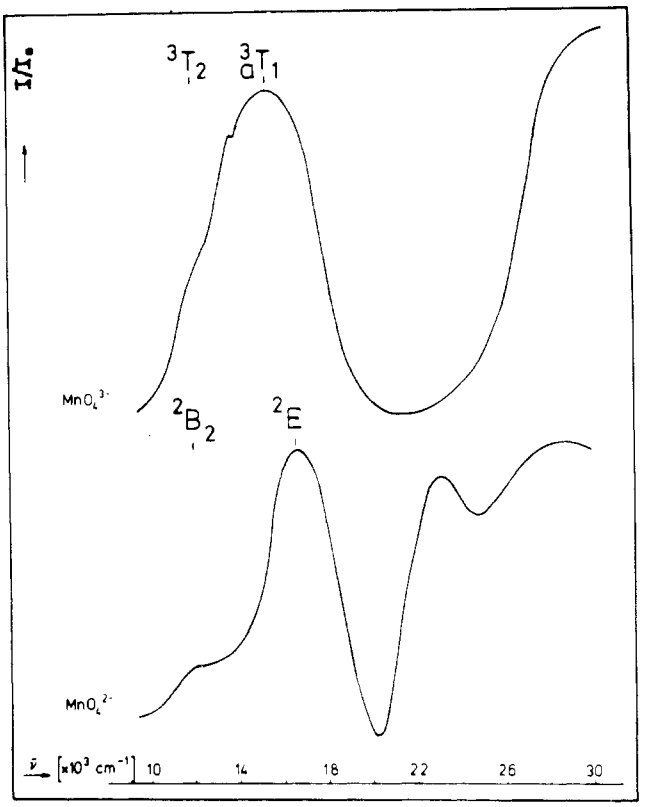

Figure 2. Spectra of tetrahedral MnO_4^{3-} ($^3A_2$ ground state; above) and MnO_4^{2-} (^2E ground state; below) entities in aqueous KOH solutions. In the latter case the Jahn–Teller splitting of the excited $^2T_2$ term is indicated.

Table II. Geometries of MO_4 Polyhedra in Spodiosite-Type Compounds $Ca_2(MO_4)Cl$ (Space Group *Pbcm*) (M: P;[12] V;[13] As[13])[a]

	M		
	P	V	As
	M–O Spacings (Å)		
M–O1 (2×)	1.550 (2)	1.711 (1)	1.690 (1)
M–O2 (2×)	1.532 (2)	1.703 (1)	1.679 (1)
	O(*i*)–M–O(*j*) Angles 2θ (deg)		
O1–M–O2′	107.3 (1)	105.9 (1)	105.3 (1)
O1′–M–O2	107.3 (1)	105.9 (1)	105.3 (1)
O2–M–O2′	107.8 (2)	105.6 (1)	105.5 (1)
O1–M–O1′	107.3 (2)	107.0 (1)	107.2 (1)
O1–M–O2	113.6 (1)	116.4 (1)	117.1 (1)
O1′–M–O2′	113.6 (1)	116.4 (1)	117.1 (1)
δ	2.7 (1)	4.5 (1)	4.9 (1)

[a] For δ see Table I.

mixed crystals $Ba_5(MnO_4)_x(PO_4)_{3-x}Cl$ on the Mn(V) concentration.[4] The color change from blue to green with increasing x is apprently caused by a red shift of the charge-transfer bands, which overlap the weak $^3A_2 \rightarrow {}_b{}^3T_1$ transition and lead to a sharp color-determining minimum in the green spectral region around 20 000 cm^{-1}, though the d–d transition energies remain nearly unchanged. The deviation of the MnO_4^{3-} geometry from T_d symmetry is rather small (Table I and below).

The ligand-field spectra of Mn(V)-doped host compounds with the spodiosite structure (Figure 3) are indicative of a lower symmetry component. The tetrahedral $^3A_2 \rightarrow {}_a{}^3T_1$ band of dominating intensity is split by about 4000 cm^{-1} for $Ca_2(MO_4)Cl$ (M = P, V, As) (Figure 4), in agreement with single-crystal electronic spectra of Mn(V)-doped $Ca_2(PO_4)Cl$.[5,6] Crystallographic data (Table II) indeed yield considerably tetragonally compressed tetrahedra of (nearly) D_{2d} symmetry. They cause large term splittings, which are somewhat reduced in magnitude, if Ca^{2+} is substituted by Sr^{2+}. Apparently the tetrahedra in the strontium compound, for which structural data are not available, are less distorted than those in the corresponding Ca spodiosites. Equivalent to the case of the apatite compounds (Figure 1) and the solution spectrum (Figure 2), the sharp feature at about 14 000 cm^{-1} has to be assigned to the $^3B_1 \rightarrow {}^1A_1$ transition. The minima have positions at $\bar{\nu} \geq 21\,000$ cm^{-1} and induce blue colors. We could prepare single-phase compounds only with Mn(V) concentrations below 5 mol %.

Table III. Geometries of MO_4 Polyhedra in Li_3PO_4[15] and Li_3VO_4[16] (Low-Temperature Phases; Space Group $Pmn2_1$) and Li_3PO_4[14] (High-Temperature Phase; Space Group *Pmnb*)[a]

	M		
	P (HT)	P (LT)	V (LT)
	M–O Spacings (Å)		
M–O1 (2×)	1.55 (2)	1.546 (5)	1.717 (1)
M–O2	1.56 (2)	1.550 (7)	1.714 (1)
M–O3	1.56 (2)	1.542 (8)	1.720 (1)
	O(*i*)–M–O(*j*) Angles 2θ (deg)		
O1–M–O1′	110.0	110.6 (3)	111.22 (5)
O1–M–O2 (2×)	110.0	109.9 (2)	110.98 (5)
O1–M–O3 (2×)	109.0	108.5 (3)	107.64 (5)
O2–M–O3	110.0	109.3 (4)	108.20 (7)
δ	0.5	0.7 (3)	1.6 (1)

[a] For δ see Table I.

Mn(V) in compounds with the $Li_3(MO_4)$ structure (M = P(V), V(V), As(V)) have greenish blue colors. The tetrahedral positions are even more regular than for the apatites (Table III), and the reflection spectra are similar to those of the apatites. Electronic spectra were first reported by Kingsley et al.[17] but were assigned differently. Li_3MnO_4 occurs in two modifications,[18] which differ only slightly and do not induce significant changes in the MnO_4^{3-} geometry. In contrast to ref 18, we observed for both phases the same green-blue colors.

The spectra in Figure 3 have been assigned and fitted with Δ_t = 11 000 ± 400 cm^{-1}, B = 500 cm^{-1}, C/B = 4.35, and ξ = 120 cm^{-1}. The D_{2d} symmetry component was accounted for by utilizing the angular overlap model, with the energy parameters e_σ = 15 000 ± 500 cm^{-1} $e_\pi = {}^1/_3 e_\sigma$ and with the tetrahedral angle taken as a fitting parameter. A qualitative diagram of the term splittings is given in Figure 4.

In summary, Mn(V) in tetraoxo coordination may induce blue and also green colors, depending on the host structure and composition as well as on the Mn(V) concentration.

Manganese(VI). Mn(VI) can be stabilized in various host compounds with the β-K_2SO_4 structure, where nearly regular tetrahedral sites are occupied. Polarized single-crystal spectra are reported for Mn(VI)-doped $BaSO_4$, $BaSeO_4$, K_2SO_4, and K_2CrO_4.[19,20] The reflection spectra in Figure 5 and the solution spectrum in Figure 2 show three transitions below 28 000 cm^{-1}, from which only the weak band around 12 000 cm^{-1} was assigned to a d–d transition ($^2E \rightarrow {}^2T_2$ in T_d) by Day et al.[20] We propose a different spectral assignment, explaining the two lowest energy bands by the presence of a strong vibronic $T_2 \times \epsilon$ coupling in the excited state, which splits the T_2 term into a lower energy B_2 and a higher energy E component (D_{2d} symmetry), yielding the transitions $^2B_1$ ($d_{x^2-y^2}$) $\rightarrow {}^2B_2$, ^2E at 12 000, 16 500 cm^{-1} (Figure

(10) Sundarsanan, K.; Young, R. A. *Acta Crystallogr.* **1974**, *B30*, 1381.
(11) Hata, M.; Marumo, F.; Iwai, S. *Acta Crystallogr.* **1979**, *B35*, 2382.
(12) Greenblatt, M.; Banks, E.; Post, B. *Acta Crystallogr.* **1967**, *B23*, 166.
(13) Banks, E.; Greenblatt, M.; Post, B. *Inorg. Chem.* **1970**, *9*, 2259.
(14) Zeeman, J. *Acta Crystallogr.* **1960**, *B13*, 863.
(15) Keffer, C.; Mighell, A.; Mauer, F.; Swanson, H.; Block, S. *Inorg. Chem.* **1967**, *6*, 119.
(16) Shannon, R. D.; Calvo, C. *J. Solid State Chem.* **1973**, *6*, 538.
(17) Johnson, P. D.; Prener, J. S.; Kingsley, J. D. *Science* **1963**, *141*, 1179.
(18) Meyer, G.; Hoppe, R. *Z. Anorg. Allg. Chem.* **1976**, *424*, 249.
(19) Ezzeh, C.; McGarvey, B. R. *J. Chem. Phys.* **1974**, *61*, 2675.
(20) DiSipio, L.; Oleari, L.; Day, P. *J. Chem. Soc., Faraday Trans. 2* **1972**, *68*, 776. Day, P.; DiSipio, L.; Ingletto, G.; Oleari, L. *J. Chem. Soc., Dalton Trans.* **1973**, *23*, 2595.

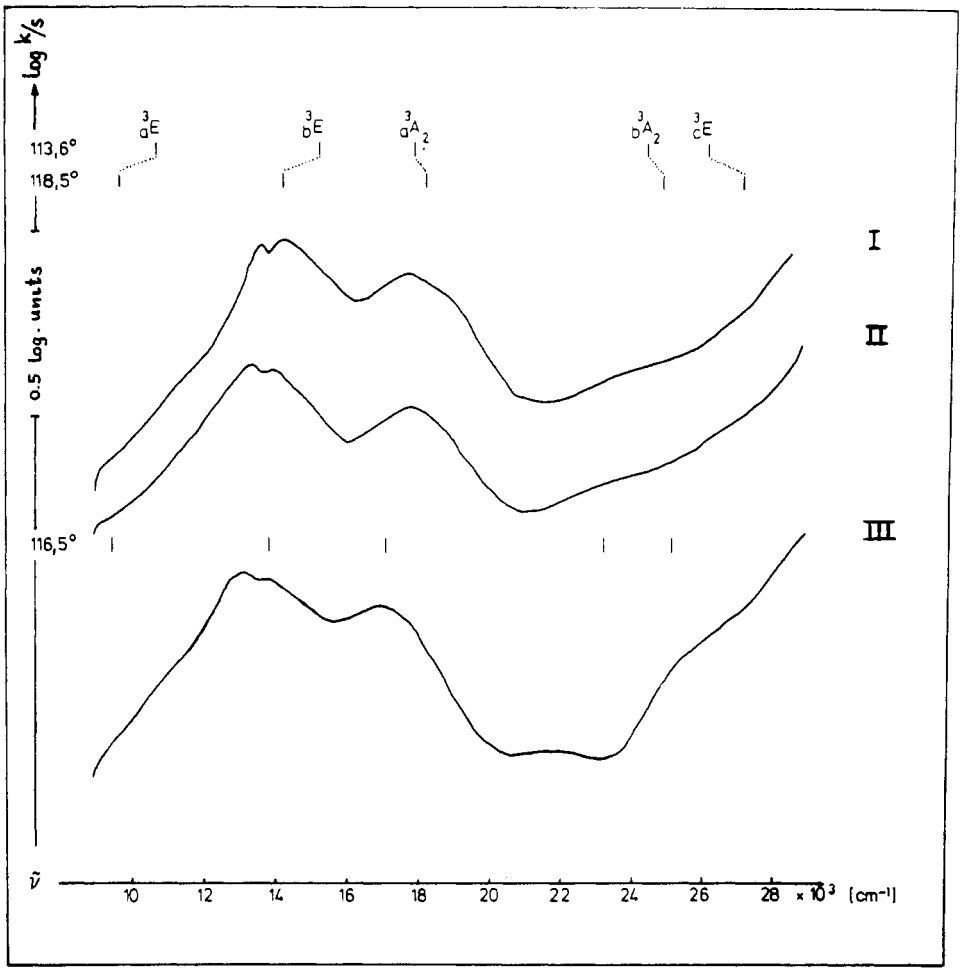

Figure 3. Reflection spectra of Mn(V)-doped (1 mol %) spodiosite-type compounds $Ca_2(PO_4)Cl$ (I), $Ca_2(VO_4)Cl$ (II), and $Sr_2(VO_4)Cl$ (III). The energies of the spin- and symmetry-allowed transitions (D_{2d}) were calculated with the parameters Δ = 11 350 (10 600) cm^{-1}, B = 500 cm^{-1} for the tetrahedral angles 113.6 and 118.5° (116.5°). (The angle 113.6° refers to the geometry of the PO_4^{3-} tetrahedra; see Table II.)

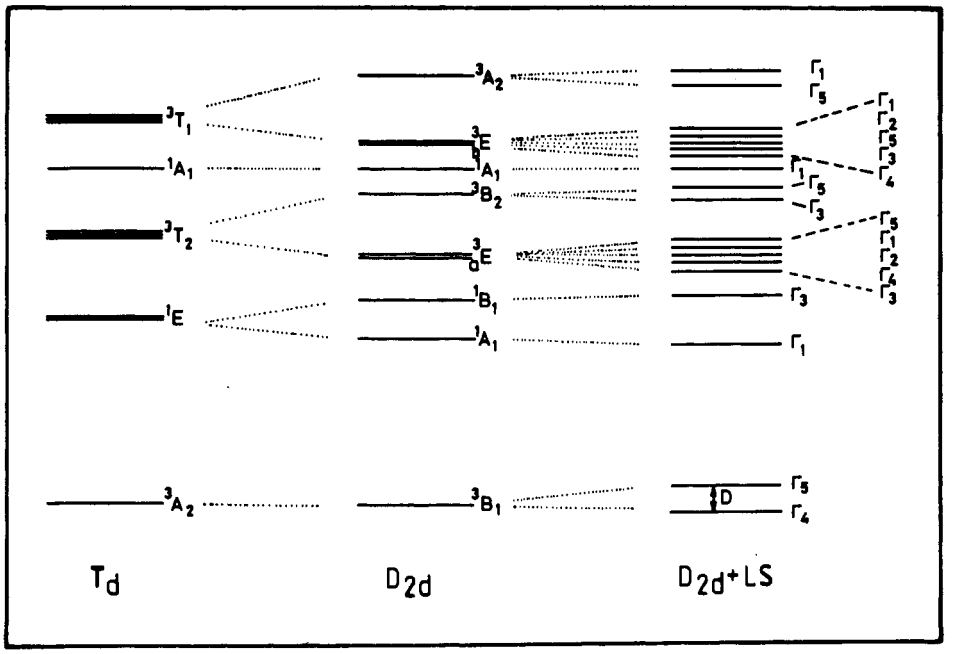

Figure 4. Term diagram of Mn(V) in T_d symmetry, in a compressed D_{2d} geometry and with the inclusion of spin–orbit coupling (schematic; only nearest excited states).

2). In accord with the observed intensities the first transition is symmetry-forbidden. A Δ parameter of ≈14 500 cm^{-1} is estimated (12 000 cm^{-1} in Day's assignment), which seems more reasonable in comparison with the Δ value of ≈11 000 cm^{-1} for Mn(V). Also, the sequence of the position of the lowest energy charge-transfer band going from Mn(V) to Mn(VI) and to Mn(VII)—namely 32 000, 24 000, 15 000 cm^{-1}—seems to be more consistent than with the first charge-transfer band for Mn(VI) at 18 000 cm^{-1}.[20] This assignment is also in accord with the spectra of the isoelectronic Cr(V) ion in the tetraoxo coordination of various host

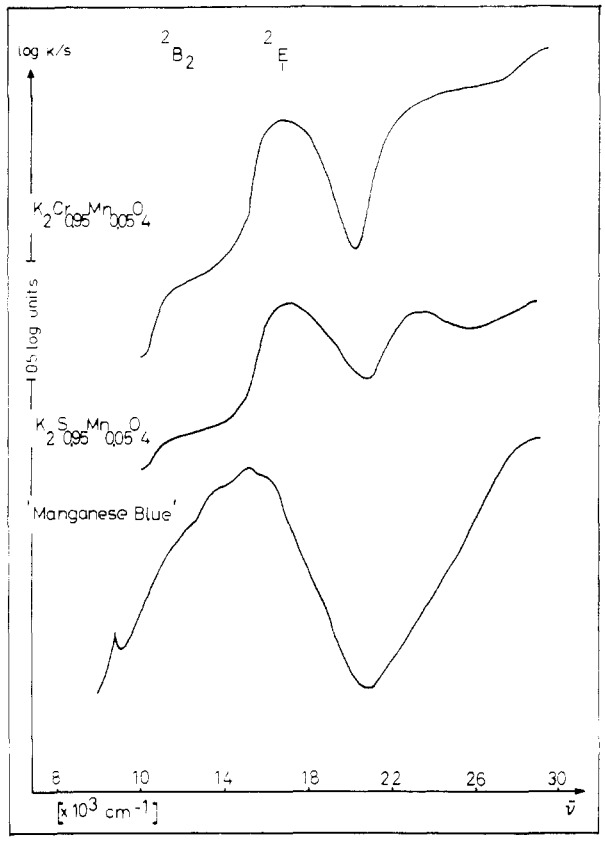

Figure 5. Reflection spectra of Mn(VI)-doped K_2CrO_4 and K_2SO_4 (band assignment as in Figure 2) and of "manganese Blue".

structures, where the first charge-transfer band occurs at 28000 cm^{-1}.[20] Hence, the assignment of the absorption in the visible region, which is widely split in analogy to the case for Mn(VI) but is observed at about 10% lower energies, to the $^2B_1$ (^2E) → $^2B_2$, ^2E ($^2T_2$) transitions is clearly established in this case. Further support comes from EPR spectroscopy,[21] which finds a $d_{x^2-y^2}$ ground-state orbital. Presumably the orbital degeneracy of the ^2E ground state is lifted by the Jahn–Teller effect, though the small lower symmetry components of the tetrahedral sites might also have induced a splitting.

The bonding situation of tetrahedral Mn(VI) resembles the one observed for octahedral Ti(III), where also a very large Jahn–Teller splitting of the excited state is observed.[22] This state is ($\sigma + \pi$) antibonding for a tetrahedral d^1 system ($^2T_2$) and purely σ antibonding (^2E_g) for an octahedral d^1 complex. In both cases the ground states ^2E and $^2T_{2g}$ are only π antibonding, and hence only small splittings due to the Jahn–Teller effect are expected.

Mn(VI)-doped K_2CrO_4 is green as the MnO_4^{2-} ion in solution, while Mn(VI)-doped K_2SO_4 is blue. The shift of the ligand-field and charge-transfer bands in the latter case is apparently due to the large difference in the ionic radii of Mn(VI) and S(VI) (≈0.2 Å), which increases the ligand field acting on Mn(VI) ($\Delta \approx 16000$ cm^{-1}; Figure 5).

In Figure 5 is also depicted the reflection spectrum of the commercial "manganese blue", which is claimed to be Mn(VI) in the host compound $BaSO_4$. The comparison with Figure 1 gives direct evidence, however, that the color center is very probably Mn(V). Indicative for Mn(V) in particular is the presence of the $^3A_2 \rightarrow {}_a{}^1E$ transition around 8500 cm^{-1}. Unfortunately the EPR spectrum is very unspecific and no confirmation of this oxidation state can be deduced from it.

B. EPR Powder Spectra. Manganese(V). The $^3A_2$ ground state of tetrahedral Mn(V) undergoes zero-field-splitting effects, if lower symmetry ligand-field components are present. The EPR spectra

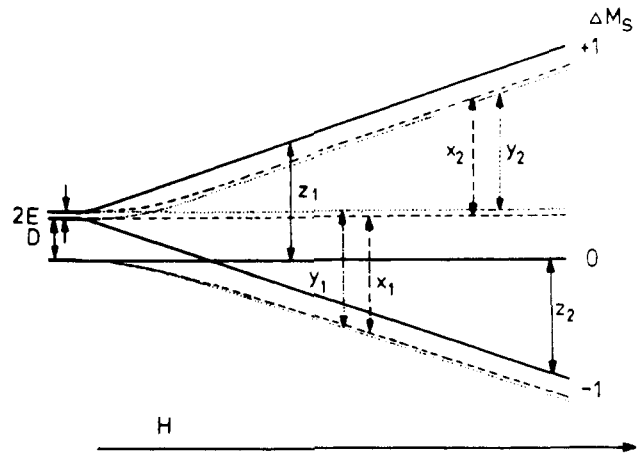

Figure 6. Zero-field splitting of a spin-triplet $^3A_2$ ground state (T_d) due to the presence of an axial distortion (D_{2d} compression; $D > 0$) with a small orthorhombic symmetry component superimposed ($E \neq 0$). The $\Delta M_s = 1$ transitions in an external magnetic field along x, y, and z are marked, with z giving the direction of compression (S_4 axis of a tetrahedron with D_{2d} symmetry).

of spin-triplet states are described by the spin Hamiltonian of eq 1 if a coordinate system is chosen where the zero-field-splitting

$$\hat{H} = \beta \hat{H} \hat{g} \hat{S} + \hat{S} \hat{D} \hat{S} \tag{1}$$

$$\hat{S}\hat{D}\hat{S} = D((\hat{S}_z^2 - \tfrac{1}{3}S(S+1)) + E(\hat{S}_x^2 - \hat{S}_y^2)$$

tensor **D** is diagonal. The D_x, D_y, and D_z components of **D** are related to the usual zero-field-splitting parameters D and E by eq 2. The six possible $\Delta M_s = 1$ transitions in a magnetic field

$$D = \tfrac{1}{2}(2D_z - D_x - D_y) \qquad E = \tfrac{1}{2}(D_x - D_y) \tag{2}$$

induced by an orthorhombic zero-field splitting are illustrated by Figure 6, and the respective energies together with those corresponding to the three $\Delta M_s = 2$ transitions are given in eq 3.[23] In

$$\begin{aligned}
aH_{x_{1(2)}}{}^2 &= (H_0 \underset{(+)}{-} D' \underset{(-)}{+} E')(H_0 \underset{(-)}{+} 2E') \\
aH_{y_{1(2)}}{}^2 &= (H_0 \underset{(+)}{-} D' \underset{(+)}{-} E')(H_0 \underset{(+)}{-} 2E') \\
aH_{z_{1(2)}}{}^2 &= (H_0 \underset{(+)}{-} D')^2 - E'^2 \\
aH_{x_{3(y_3)}}{}^2 &= \tfrac{1}{4}(H_0^2 - (D' \underset{(-)}{+} E')^2) \\
aH_{z_3}{}^2 &= \tfrac{1}{4}(H_0^2 - 4E'^2)
\end{aligned} \tag{3}$$

powder spectra two further transitions may be observed.[23] H_{min} characterizes the low-field limit of the spectrum, while H_{dq} corresponds to a double-quantum absorption:

$$\begin{aligned}
aH_{min}{}^2 &= \tfrac{1}{4}H_0^2 - \tfrac{4}{3}(D'^2 + 2E'^2) \\
aH_{dq}{}^2 &= H_0^2 - \tfrac{1}{3}D'^2 - E'^2
\end{aligned} \tag{4}$$

H_0 is defined by $h\nu = g_0 \beta H_0$ (ν is microwave frequency; β is the Bohr magneton), and the coefficient a is the ratio g^2/g_0^2. The zero-field-splitting parameters $D(E)$ in wavenumbers are related to $D'(E')$ by $D(E) = D'(E')\nu/cH_0$.

The **g** tensor was regarded as isotropic because the orbital contributions (deviation of g from the spin-only value g_0) are very small (eq 5).

$$g = g_0 - 4\xi/\Delta \qquad (\xi = k^2\xi_0) \tag{5}$$

EPR powder spectra of Mn(V)-doped oxidic compounds with the spodiosite structure taken under Q-band conditions (Figure 7) are well resolved and show besides H_{min} all $\Delta M_s = 1$ transitions.

(21) Carrington, A.; Ingram, D. J. E.; Lott, K. A. K.; Schonland, D. S.; Symons, M. C. R. *Proc. R. Soc. London* **1960**, *A254*, 101.
(22) Ameis, R.; Kremer, S.; Reinen, D. *Inorg. Chem.* **1985**, *24*, 2751.
(23) Wasserman, E.; Snyder, L. C.; Yager, W. A. *J. Chem. Phys.* **1964**, *41*, 1763.

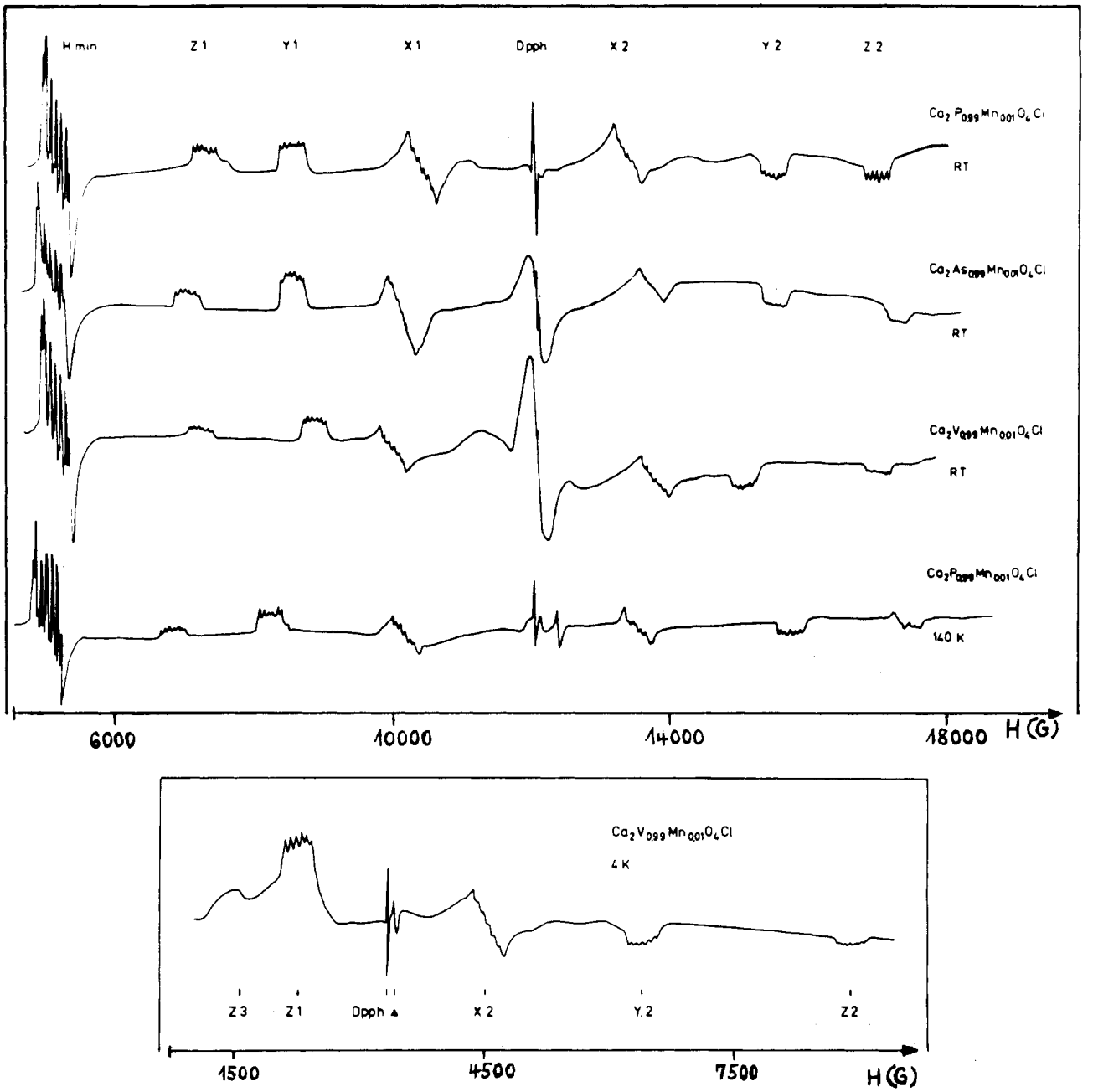

Figure 7. EPR powder spectra of Mn(V)-doped compounds with the spodiosite structure under Q-band (ν = 34.8 GHz; room temperature and 140 K; above) and X-band conditions (ν = 9.05 GHz; 4 K; below).

In the X-band spectra, which were sufficiently intense and resolved only below 77 K (Figure 7), some transitions are not present anymore, due to the lower observation frequency. The broad signal at $g \approx 1.97$ very near the DPPH standard and the narrow signal at $g = 1.94$ in the low-temperature spectra will be discussed below. The manganese hyperfine structure is nicely seen in all signals and yields $A = 58 \pm 1 \times 10^{-4}$ cm^{-1}, consistent with reported $|A|$ values for Mn(IV) in oxidic coordination (71×10^{-4} cm^{-1}, octahedral) and Mn(II) (81×10^{-4} cm^{-1}, octahedral; 75×10^{-4} cm^{-1}, tetrahedral).[24] The spectra of Mn(V)-doped compounds with the Li_3PO_4 structure are less resolved and the D and E parameters considerably smaller. The hyperfine splitting is the same as for the spodiosite-type compounds.

In Table IV the zero-field-splitting parameters derived from the powder spectra are collected, supplemented by data for compounds with the apatite structure.[4] D is $0.45_5 \pm 0.01_5$ cm^{-1} (298 K) for the Mn(V)-doped Ca^{2+} compounds with the spodiosite structure and is about 10% larger at low temperatures. Because the tetrahedral site symmetry is nearly D_{2d}, with only a small lower symmetry component superimposed (Table II), the orthorhombicity parameter E is rather small. D varies only slightly going from the phosphate to the arsenate and vanadate, though the tetrahedra in the two latter compounds show a much larger deviation from T_d geometry than the PO_4^{3-} polyhedra (Table II). Apparently the MnO_4^{3-} polyhedra are sterically not significantly influenced by the host tetrahedra but create their own individual geometry. Because the Mn–O spacing is 1.70 Å[4] and hence is nearly identical with the V–O and As–O bond lengths (Table II), one may suggest that the MnO_4^{3-} geometry is similar to the ones of VO_4^{3-} and AsO_4^{3-} in the Ca^{2+} spodiosites.

Figure 4 illustrates that the zero-field splitting is induced by the interaction of the otherwise energetically degenerate Γ_4 and Γ_5 L–S components of the $^3A_2$ ground state with corresponding split states of the excited $^3T_2$ states via spin–orbit coupling. In a first approximation, one may restrict oneself to the interaction with the first excited state $^3T_2$:[24]

$$D \simeq \xi^2 \delta E / \Delta^2 \qquad (6)$$

In this approximation the parameter D is directly related to the

(24) Abragam, A.; Bleaney, B. *Electron Paramagnetic Resonance of Transition Ions*; Clarendon Press: Oxford, U.K., 1970; pp 432, 440, 450.

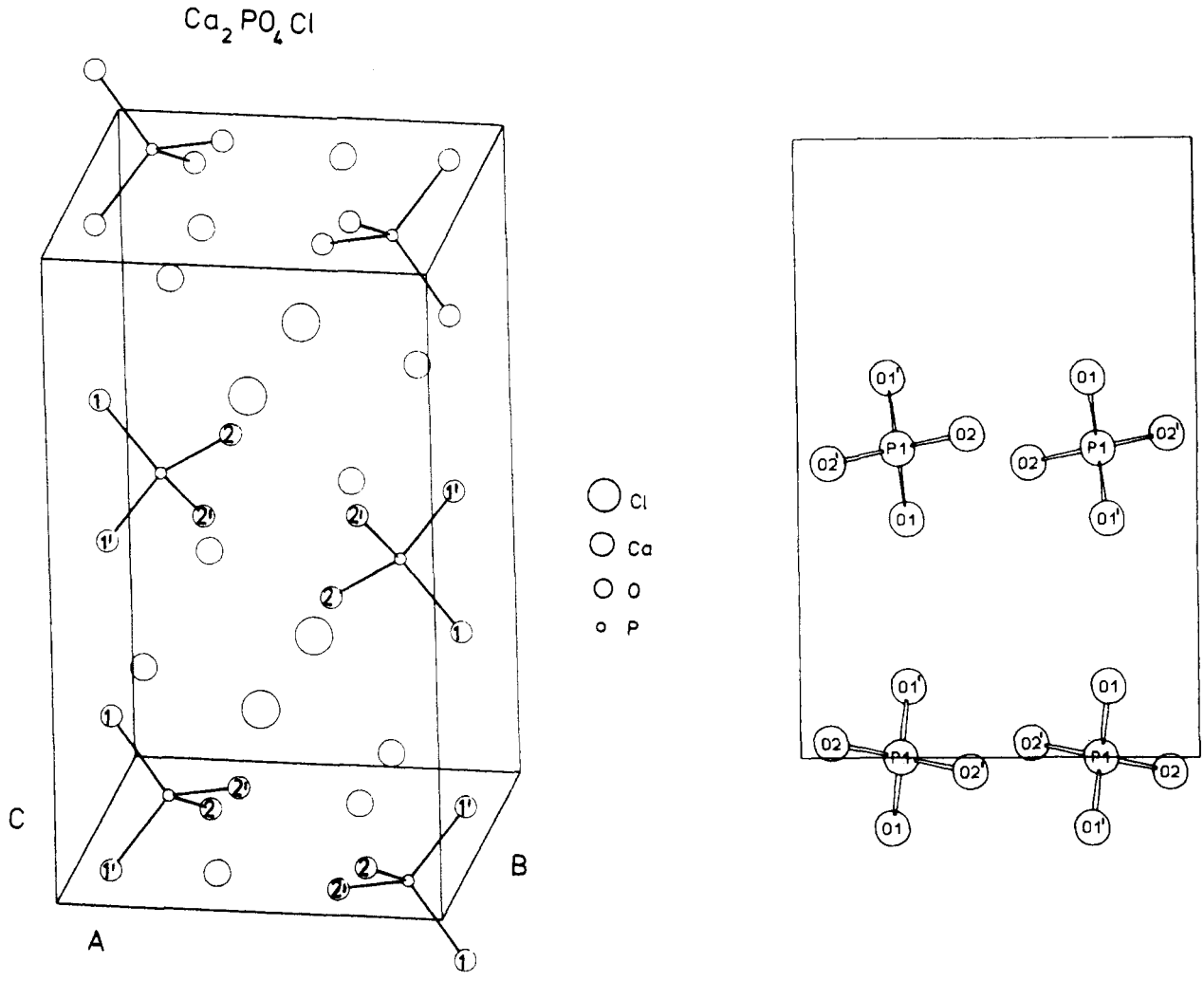

Figure 8. Orthorhombic unit cell of $Ca_2(PO_4)Cl$ with the spodiosite structure (left) and the projection of the PO_4^{3-} polyhedra into the *b*–*c* plane (right).

Table IV. Zero-Field-Splitting Parameters (cm^{-1}) for Mn(V) in Oxidic Solids with the Li_3PO_4, Apatite, and Spodiosite Structures Derived from EPR Powder Spectra with $g = 1.96$ (1) (Eq 3 and 4; X- and Q-Band Data)

compd	x^a	band	T, K	D	E
Li_3PO_4	1	Q	298	0.17	0.00
		X	4	0.14	0.01
Li_3AsO_4	1	Q	298	0.17	0.01
		X	4	0.17	0.01
Li_3VO_4	1	Q	298	0.25	0.03
		X	4	0.22	0.01
$Ba_5(PO_4)_3Cl$	1	Q	298	0.44_3	0.05_5
		Q	130	0.46_7	0.06_4
		X	4	0.47	0.06_5
$Sr_5(PO_4)_3Cl$	0.5	Q	298	0.36_9	0.04_5
		Q	130	0.43_9	0.05_3
		X	4	0.44	0.06
$Ca_2(PO_4)Cl$	1	Q	298	0.44_3	0.06_2
		Q	130	0.48_7	0.06_3
$Ca_2(AsO_4)Cl$	1	Q	298	0.47_0	0.05_3
$Ca_2(VO_4)Cl$	1	Q	298	0.45_7	0.03_7
		X	4	0.50_1	0.04_3
$Sr_2(VO_4)Cl$	1	X	4	0.25_8	0.01_9

[a] Mole percent Mn(V) in tetrahedral sites.

tetragonal splitting of the $^3A_2 \rightarrow {}^3T_2$ transition ($\delta E = E(^3B_2) - E(^3E)$) and has a positive sign (Γ_5 above Γ_4) for axially compressed Mn(V) tetrahedra. If one anticipates, that the doped MnO_4^{3-} tetrahedra adopt essentially the geometry of the host polyhedra (see below), D should be positive for the spodiosite compounds. The effective L–S coupling parameter ξ can be estimated from the experimental g value ($1.96 \triangleq 0.01$; Table IV) and $\Delta \simeq 11\,000$ cm^{-1} (eq 5) to be $\simeq 120$ cm^{-1} ($\xi_0 \simeq 440$ cm^{-1}, extrapolated from the free-ion ξ_0 values for Mn(0) up to Mn(IV);[25] $k \simeq 0.52$), yielding $\delta E \approx 4000$ cm^{-1} for $D = 0.45$ cm^{-1}. This value correlates reasonably well with the one of 4500 cm^{-1}, which was obtained by fitting the experimental electronic spectra of Mn(V)-doped $Ca(M^VO_4)_2Cl$ spodiosites (M^V = P, As, V) with $2\theta = 118.5°$ and $\Delta = 11\,350$ cm^{-1} (Figure 3)—corresponding to a considerable tetragonal compression of the MnO_4^{3-} tetrahedra along a (pseudo) S_4 axis. This result confirms the presence of MnO_4^{3-} tetrahedra, which are compressed to an even larger extent than the VO_4^{3-} and AsO_4^{3-} polyhedra (Table II), in all three host compounds. For an angle of 113.6°, which characterizes the PO_4^{3-} tetrahedra in $Ca_2(PO_4)Cl$ (Table II), a much smaller splitting of the symmetry-allowed $^3A_2 \rightarrow {}^3T_1$ band ($\simeq 2000$ cm^{-1}) is expected than is actually observed ($\simeq 4500$ cm^{-1}) (Figure 3). The substitution of Ca^{2+} by Sr^{2+} reduces the distortion, as can be deduced from the ligand-field spectrum (Figure 3). From the comparison of calculated and experimental band energies, a 2θ angle of $\simeq 116.5°$ is estimated.

The zero-field-splitting parameters of Mn(V)-doped compounds Li_3MO_4 (M = P, As, V) (Table IV) are considerably smaller, in accord with the structural data, which indicate nearly undistorted tetrahedra (Tables III). In this host structure (in contrast to the spodiosite lattice) the difference in the extent of the tetrahedral distortion between P(V) and V(V) compound is reflected by the D values. Presumably, the cooperative-elastic interactions between the MO_4^{3-} polyhedra are larger in this case because they are connected via the small Li^+ ions, which have a stronger polarizing

(25) Griffith, J. S. *The Theory of Transition Metal Ions*; Cambridge University Press: Cambridge, U.K., 1971; p 437.

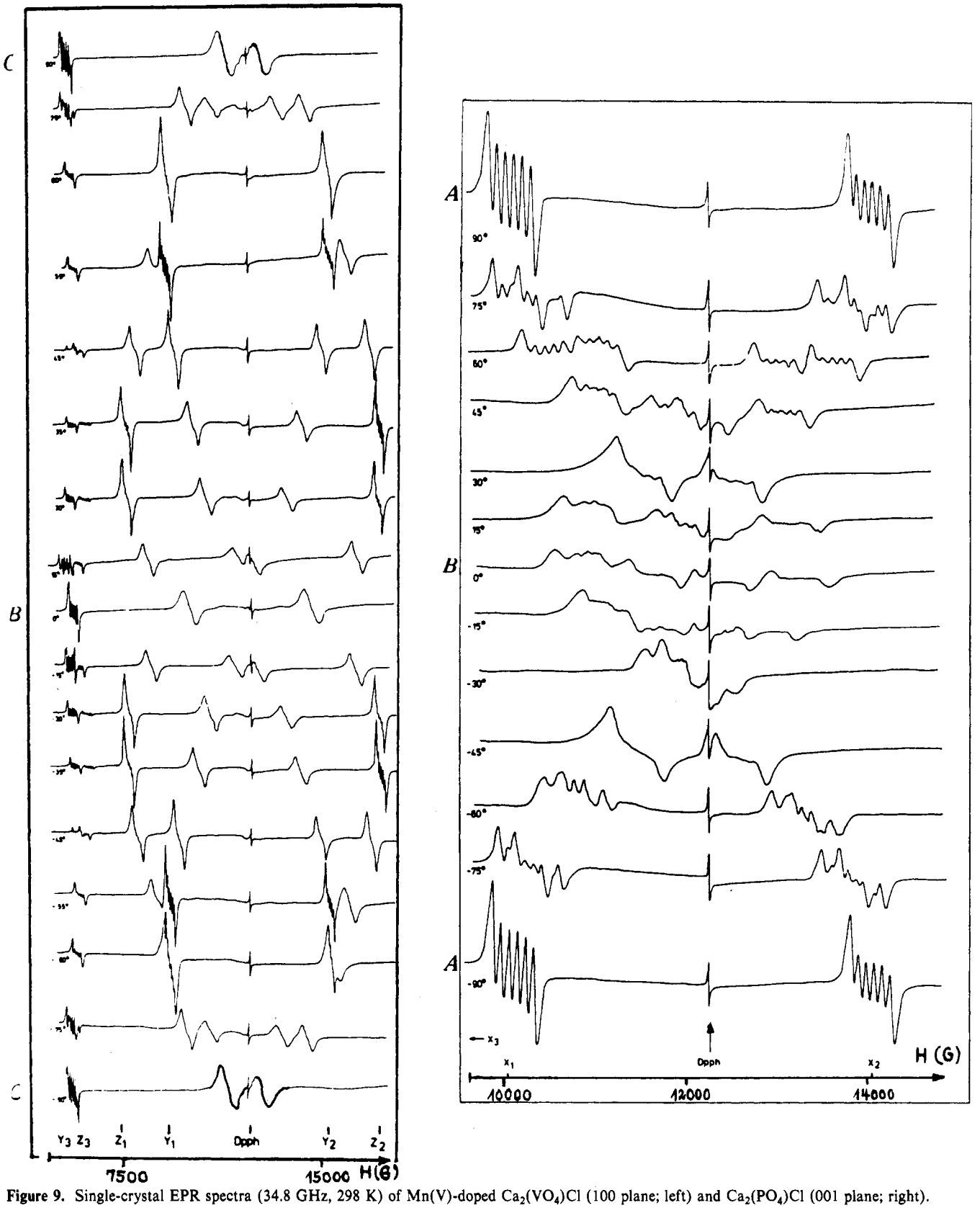

Figure 9. Single-crystal EPR spectra (34.8 GHz, 298 K) of Mn(V)-doped $Ca_2(VO_4)Cl$ (100 plane; left) and $Ca_2(PO_4)Cl$ (001 plane; right).

power than Ba^{2+}, Sr^{2+}, or even Ca^{2+}.

The EPR data for Mn(V) in compounds with the apatite structure are discussed elsewhere,[4] and only one argument will be given here. The tetrahedra in this structure type are distorted along a C_3 axis (C_{3v} symmetry in the first approximation). Though the deviation from the T_d geometry is considerably smaller than for the spodiosite type Ca^{2+} compounds (Tables I and II), the zero-field-splitting parameters are of comparable magnitude (Table IV). This is due to the fact, that eq 6 has to be supplemented by a second interaction term of about the same magnitude in case of axial fields of trigonal symmetry.[24]

The additional EPR signals in the powder EPR spectra (Figure 7) presumably originate from exchange narrowing due to Mn–Mn interactions. It has indeed been demonstrated for $Ba_5(PO_4)_{5-x}(MnO_4)_xCl$ mixed crystals that—going from doped crystal powders to $x = 3$—the triplet spectrum gradually collapses into one signal at $g \approx 1.97$.[4] Besides this strong signal, only a very weak half-field signal (H_{min}) remains.

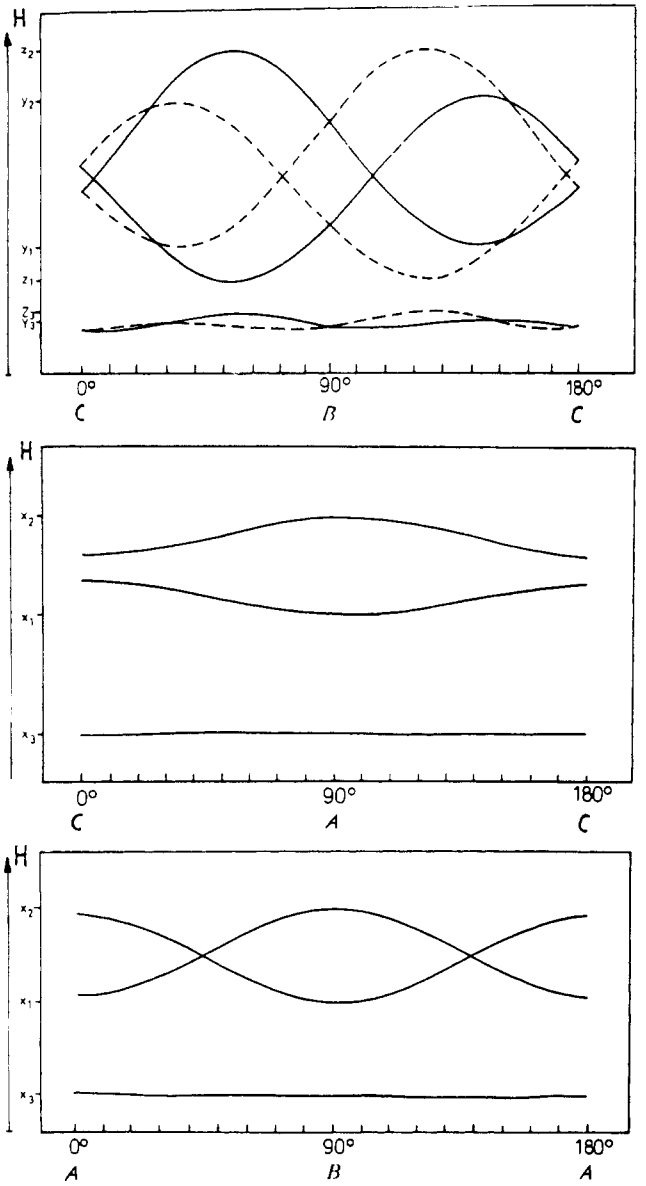

Figure 10. Angular dependencies (schematic) of the **D** tensor for Mn(V)-doped $Ca_2(MO_4)Cl$ [M = V(V), As(V)] in the (100), (010), and (001) planes. The two differently oriented MO_4 polyhedra are indicated in the (001) plane; fitting curves are calculated with $D' = 4500$ G, $E' = 550$ G, $g = 1.97$, and $\nu = 34.8$ GHz. (For the magnetic field scales and the experimental values in the *BC* plane see Figure 9; the agreement between experimental values and fitting curves is similar to the one in Figure 10.)

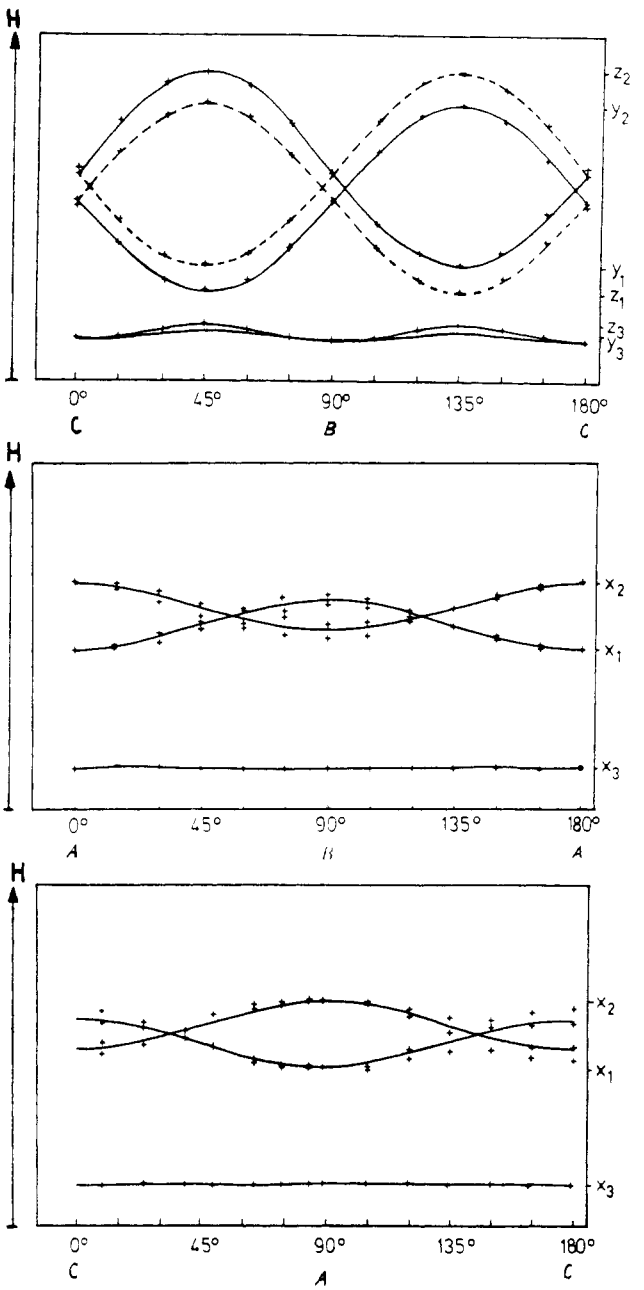

Figure 11. Angular dependencies of the **D** tensor for Mn(V)-doped $Ca_2(PO_4)Cl$ in the (100), (001), and (010) planes. The two differently oriented MO_4 polyhedra are indicated in the (001) plane; fitting curves use the parameters of Figure 10 (for magnetic field scale, see Figure 9).

Manganese(VI). Due to the d^1 configuration and deviations of the Mn(VI) polyhedron from the regular T_d symmetry (either by the imposed host site geometry or by vibronic coupling effects of the Jahn–Teller type), usually a broad EPR signal at $g = 1.96 \pm 0.02_5$ is observed for Mn(VI)-doped $BaSO_4$, $BaSeO_4$, K_2SO_4, K_2SrO_4, etc. that is resolved into the orthorhombic components at 4.2 K.[19,21,26] It is not particularly characteristic for the identification of Mn(VI) because Mn(V) induces a signal at the same g value in the case of exchange-narrowed EPR spectra.

C. EPR Single-Crystal Results. Manganese(V). The orientations of the **D** tensor components in spodiosite type compounds were determined by single-crystal EPR measurements in the three mutually perpendicular planes *ab*, *bc*, and *ca* (space group *Pbcm*). From the four tetrahedra in the unit cell (Figure 8) two are magnetically inequivalent. The two molecular C_2 (pseudo-S_4) axes are inclined by 72° toward each other and are oriented perpendicular to the crystallographic *a* direction in the case of the MO_4^{3-} entities in $Ca_2(MO_4)Cl$ (M = P(V), As(V), V(V)).[12-14] They have angles of ±36 and ±54° with respect to *b* and *c*.

Single crystals of the Mn(V)-doped compounds with the approximate dimensions $1.3 \times 0.45 \times 0.3$ mm^3 were selected. Nicely resolved spectra are observed already at 298 K, which are characteristic for the presence of two Mn(V) centres (Figure 9). It is immediately evident from the angular dependencies of the **D** tensor for the compounds with M = V(V), As(V) that the D_z, D_y, and D_x components (eq 2) follow closely the (approximate) D_{2d} symmetry of the tetrahedra (Figure 10, Table IV). While D_z (=0.28 cm^{-1}) is aligned parallel to the pseudo-S_4 axis, D_y (−0.19 cm^{-1}) and D_x (−0.09 cm^{-1}) are correlated with the two pseudo-C_2 directions. One of the latter axes has the direction of *a* (D_x).

In Figure 11 are depicted the angular dependencies of the **D** tensor for Mn(V)-doped $Ca_2(PO_4)Cl$. Small misadjustments in the single-crystal orientation explain the slight inconsistencies in the (010) and (001) planes. It is interesting, that the two D_z directions have changed the orientation with respect to Figure 10,

(26) Greenblatt, M.; Pifer, J. H. *J. Chem. Phys.* **1980**, *72*, 529.
(27) Kosky, C. A.; McGarvey, B. R. *J. Chem. Phys.* **1972**, *56*, 5904.

having here angles of ±45° with the crystallographic *b* and *c* axes. The C_2 (pseudo-S_4) axes of the two magnetically inequivalent Mn(V) polyhedra are now perpendicular with respect to one another. While the MnO_4^{3-} polyhedra adapt the geometry and orientation of the host tetrahedra in the vanadate and arsenate without significant changes, this is apparently not so for the phosphate. Not only is the extent of the compression much larger than the one that characterizes the PO_4^{3-} tetrahedra in $Ca_2(PO_4)Cl$ (Tables II and IV), but also the orientation of the MnO_4^{3-} tetrahedra seems to be different (by ≈10°) from those of the PO_4^{3-} entities, which may be explained by packing forces due to the considerably larger ionic radius of Mn(V) compared to P(V).

Single-crystal EPR measurements were also performed with various apatite-type compounds. We were not able to analyze the angular dependencies of the **D** tensor, however. Presumably D_z, D_y, and D_x do not follow the approximate C_{3v} symmetry of the three magnetically inequivalent MO_4^{3-} polyhedra in the unit cell.

Conclusions and Summary

Strong d–d bands for both Mn(V) and Mn(VI) in tetrahedral oxo coordination are found around 16 000 cm^{-1} (Figure 2). Though the two spectra are quite different in their special features, a charge-transfer band is present at about 24 000 cm^{-1} for Mn(VI), while there is no significant absorption at these wavenumbers for Mn(V). At higher Mn(V) concentrations charge-transfer bands may move into the visible region also in this case. Both cations may induce green and blue colors. The color-determining minimum can be shifted from ≈20 000 cm^{-1} (green) to ≈22 000 cm^{-1} (blue) by geometric packing effects (compression due to small host site cations), by symmetry reduction (splittings and broadening of bands in the visible region), and by varying the concentration of manganese in the host compound.

Mn(V) and Mn(VI) can easily be distinguished by their EPR spectra in crystalline compounds with low doping concentrations, because well-resolved triplet transitions are observed for the d^2 configuration. At higher manganese concentrations, however, the triplet spectrum collapses to one signal at $g \approx 1.96$ as the consequence of exchange interactions. Because the half-field signal (H_{min}) is very weak in these cases and Mn(VI) induces an EPR signal also at $g \approx 1.96$, a discrimination between the two oxidation states may be difficult.

The EPR triplet spectra of Mn(V) together with the ligand spectra have been shown to be very informative with respect to the electronic ground state and the geometry and the volume of the MnO_4^{3-} polyhedron in the respective host compound. It was possible to derive from the single-crystal EPR spectra of various spodiosite-type compounds the specific differences in the geometry and the polyhedron orientation of the MnO_4^{3-} entities in comparison to the host tetrahedra. Thus, in the $Ca_2(PO_4)Cl$ host structure the S_4 directions of the two magnetically inequivalent MnO_4^{3-} polyhedra are oriented perpendicular to each other, compared to the angle of 72° between the PO_4^{3-} host polyhedra. Besides this misorientation of about 10°, the MnO_4^{3-} polyhedra exhibit a comparatively much stronger flattening than the PO_4^{3-} entities. Both effects are due to the considerably larger ionic radius of Mn(V) with respect to P(V) (Table I)[4] and presumably induced by packing forces in the unit cell.

Acknowledgment. Financial support by the Deutsche Forschungsgemeinschaft and the Fonds der chemischen Industrie is gratefully acknowledged.

Registry No. $Ca_2(PO_4)Cl$, 12013-61-5; $Ca_2(VO_4)Cl$, 12350-23-1; $Ca_2(AsO_4)Cl$, 12523-00-1; $Sr_2(VO_4)Cl$, 12410-18-3; Li_3VO_4, 15593-56-3; Li_3AsO_4, 13478-14-3; Li_3PO_4, 10377-52-3; $Ba_5(PO_4)_3Cl$, 12356-32-0; $Sr_5(PO_4)_3Cl$, 11088-40-7; Mn, 7439-96-5.

Contribution from the Institut für Physikalische und Theoretische Chemie, Universität Regensburg, D-8400 Regensburg, Federal Republic of Germany, and Institute of Inorganic Chemistry, University of Fribourg, CH-1700 Fribourg, Switzerland

Spectroscopic Studies of Cyclometalated Platinum(II) Complexes: Optical Absorption and Emission of Single-Crystal *cis*-Bis(benzo[*h*]quinolinato)platinum(II)

R. Schwarz,[†] G. Gliemann,*[,†] Ph. Jolliet,[‡] and A. von Zelewsky*[,‡]

Received August 30, 1988

The influence of temperature (1.9 K ≤ *T* ≤ 60 K) and high magnetic fields (0 ≤ *H* ≤ 6 T) on the optical properties of single-crystal *cis*-bis(benzo[*h*]quinolinato)platinum(II) (=[Pt(bhq)$_2$]) is reported. The analysis of the polarized optical absorption and emission spectra and of the excitation spectra indicates the existence of distinct X-traps, each being provided with two electronic excited states situated energetically below the lowest exciton band. At *T* = 1.9 K a luminescence of sharp-lined structure has been observed that is a superposition of the emissions from the respective lowest excited states of the traps. Increasing temperature depopulates these states and repopulates intermediately the trap states of higher energy and finally the exciton bands, resulting in an additional fine structure and a fictitious blue shift of the emission, respectively. When a magnetic field **H**∥*b* (**H** = magnetic field vector, *b* = crystallographic *b* axis) is raised from *H* = 0 to *H* = 6 T, the intensity of the luminescence with polarization **E**∥*b* (**E** = electric field vector) increases by a factor of ~2. This result is explained by a magnetic field induced mixing of the two excited states of each trap. For **H**⊥*b* a strongly field-dependent nonradiative deactivation competes with the luminescence.

Introduction

Recently the optical properties of the cyclometalated homoleptic d^8 complexes [Pt(phpy)$_2$] (phpy = 2-phenylpyridinato) and [Pd(bhq)$_2$] (bhq = benzo[*h*]quinolinato) have been reported.[1,2]

Single-crystal [Pt(phpy)$_2$] exhibits an unstructured luminescence band. The energy and intensity of the luminescence depend on temperature and on the strength of an applied magnetic field, similar to the behavior that has been found for numerous cyanoplatinates(II),[3-8] binuclear platinum(II) complexes,[9] and tungsten pentacarbonyl crystals.[10] The experimental results could be explained by a model based on the existence of dimeric units (Pt–Pt distance 3.53 Å) in the solid state and the MLCT character

[†] Universität Regensburg.
[‡] University of Fribourg.

(1) Bär, L.; Gliemann, G.; Chassot, L.; von Zelewsky, A. *Chem. Phys. Lett.* **1986**, *123*, 264.
(2) Schwarz, R.; Gliemann, G.; Chassot, L.; von Zelewsky, A. *Inorg. Chem.*, in press.
(3) Hidvegi, I.; von Ammon, W.; Gliemann, G. *J. Chem. Phys.* **1982**, *76*, 4361.
(4) Hidvegi, I.; von Ammon, W.; Gliemann, G. *J. Chem. Phys.* **1984**, *80*, 2837.
(5) Dillinger, R.; Gliemann, G.; Pfleger, H. P.; Krogmann, K. *Inorg. Chem.* **1983**, *22*, 1366.
(6) Biedermann, J.; Wallfahrer, M.; Gliemann, G. *J. Lumin.* **1987**, *37*, 323.
(7) Schwarz, R.; Lindner, M.; Gliemann, G. *Ber. Bunsen-Ges. Phys. Chem.* **1987**, *91*, 1233.

0020-1669/89/1328-1053$01.50/0